LASER APPLICATIONS AND OTHER TOPICS IN QUANTUM ELECTRONICS PACS numbers: 42.55.Px; 42.81.Wg; 42.65.Tg
DOI: 10.1070/QE2005v035n10ABEH004003

Study of the intensity noise and intensity modulation in a of hybrid soliton pulsed source

N. Dogru, M.S. Ozyazici

***Abstract*. The relative intensity noise (RIN) and small-signal intensity modulation (IM) of a hybrid soliton pulsed source (HSPS) with a linearly chirped Gaussian apodised fibre Bragg grating (FBG) are considered in the electric-field approximation. The HSPS is described by solving the dynamic coupled-mode equations. It is shown that consideration of the carrier density noise in the HSPS in addition to the spontaneous noise is necessary to analyse accurately noise in the mode-locked HSPS. It is also shown that the resonance peak spectral splitting (RPSS) of the IM near the frequency inverse to the round-trip time of light in the external cavity can be eliminated by selecting an appropriate linear chirp rate in the Gaussian apodised FBG.**

Keywords: *mode-locked laser, intensity modulation, spontaneous noise, carrier density noise, relative intensity noise, multiquantum well laser, external cavity laser, hybrid soliton pulse source, fibre Bragg grating, resonance peak spectral splitting.*

1. Introduction

A variety of applications ranging from optical communications to radar systems require picosecond optical pulses at a high repetition rate. Active mode-locking with external cavity gratings is used to generate such pulses from semiconductor lasers by injecting an alternating current at the frequency matching the round-trip time in the laser cavity. Mode-locking of external cavity lasers is a well-developed technique providing the generation of picosecond and subpicosecond pulses.

When using an external cavity configuration it is desirable to have high reflectivity at the output facet of the semiconductor laser and very low reflectivity at its inner facet for coupling to to the external cavity. Fibre grating external cavity lasers have been experimentally demonstrated in the mode-locking regime at 2.5 GHz [1] and 10 GHz [2]. Small-signal intensity modulation (IM) responses of these lasers have been described in [3 – 5]. A hybrid soliton pulse source (HSPS) is one of such devices, developed as a pulsed source for soliton transmission systems. The interesting features of these devices are the extremely wide operating frequency range, which can be extended by using chirped gratings, as reported in [6], and the relative intensity noise (RIN) investigated in [7, 8]. Analysis performed in [7, 8] included only the spontaneous emission noise sources.

In this paper, we take into account the carrier noise source in the carrier density rate equations along with the spontaneous noise and demonstrate the importance of this noise source. We also consider the small-signal IM response of a HSPS with a linearly chirped Gaussian apodised fibre Bragg grating (FBG). It was shown in [3 – 5] that a change in some parameters of a HSPS leads to an increase in the resonance peak spectral splitting (RPSS) in the IM spectra. However, our simulation results show that, RPSS can be removed by using the linear chirp rate. Here, we investigate this effect and the influence of the FBG and laser diode parameters on the IM response of the HSPS.

N. Dogru, M.S. Ozyazici Department of Electrical and Electronics Engineering, University of Gaziantep, 27310 Gaziantep, Turkey; e-mail: dogru@gantep.edu.tr

Received 4 March 2005
Kvantovaya Elektronika **35** (10) 962 – 970 (2005)
Submitted in English

2. The Model

The HSPS with a linearly chirped FBG studied in the paper is shown schematically in Fig. 1. The geometry is same as the one reported in [7, 8]. The active waveguide section has a 90 % high reflection coating (HR) on the rear facet and 1 % antireflection coating (AR) on the front facet. The fibre has a lens-like end to couple light from the laser diode and an integrated Bragg reflector served to form an external cavity with the length corresponding to the fundamental frequency of 2.5 GHz. The field in this system travels between the HR coated laser end and the effective cavity length of the grating. Power is extracted through the FBG.

We assume that the longitudinal variation in the effective index of the FBG along the propagation direction is described by the expression

$$n(z) = n_{\rm co} + \Delta n_{\rm gr}\left[1 + m\cos\left(\frac{2\pi}{\Lambda(z)}z\right)\right], \qquad (1)$$

where $n_{\rm co}$ is the unperturbed effective index of the fibre; $\Delta n_{\rm gr}$ is the refractive index change spatially averaged over the grating period; m is the modulation index of the grating. The grating period $\Lambda(z)$ is linearly chirped,

$$\Lambda(z) = \Lambda_0 + \frac{1}{2n_{\rm co}}\frac{{\rm d}\lambda_0}{{\rm d}z}z, \qquad (2)$$

where $\Lambda_0 = \lambda_0/2n_{\rm co}$ is the pitch of the unchirped Bragg

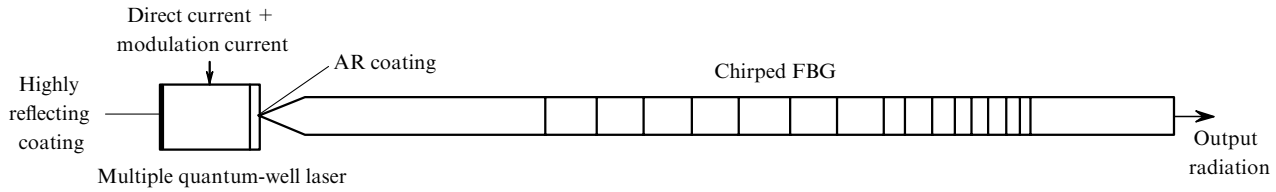

Figure 1. Scheme of a HSPS.

grating at the operating wavelength λ_0. The derivative of $d\lambda_0/dz$ with respect to z determines the chirp rate C, which is usually expressed in nm cm^{-1}.

By using the coupled-mode theory [9], the relations between the fields propagating in the forward $F(t,z)$ and backward $R(t,z)$ directions in the resonator can be written in the form

$$-\frac{dF}{dz}-i\left(\delta+\frac{2\kappa(z)}{m}-\frac{1}{2}\frac{d\varphi}{dz}\right)F=i\kappa(z)R, \tag{3}$$

$$\frac{dR}{dz}-i\left(\delta+\frac{2\kappa(z)}{m}-\frac{1}{2}\frac{d\varphi}{dz}\right)R=i\kappa(z)F. \tag{4}$$

Here, δ is the deviation of the propagation constant β from the Bragg condition ($\delta=\beta-\beta_0=\beta-\pi/\Lambda_0$); $\kappa(z)$ is the variable coupling coefficient; and

$$\varphi=-\frac{4\pi n_{co}}{\lambda_0^2}Cz^2 \tag{5}$$

is the chirp parameter.

The expression in the parentheses in Eqns (3) and (4) is called the constant 'self-coupling' coefficient [10]

$$\sigma=\delta+\frac{2\kappa(z)}{m}-\frac{1}{2}\frac{d\varphi}{dz}. \tag{6}$$

To calculate the lasing regime, spontaneous noise is added into Eqns (3) and (4) [7, 8]. The second and third terms in Eqn (6) are the gain and loss of a laser diode $\frac{1}{2}[-g(z,t)+\alpha_{las}]$, and $\delta=2\pi\Delta n/\lambda_0$, where Δn is the change in the refractive index of the laser medium caused by a change in the carrier density (see below).

The coupled-mode equations are solved by the a piecewise continuous method. The grating is divided into M sections of equal length Δz and the equations are solved analytically in each of the sections. The boundary conditions are $F(L/2)=1$ and $R(L/2)=0$ for $z=L/2$, the calculations are performed from the output to input (from $z=L/2$ to $-L/2$), and the parameters of each section are calculated and substituted into the 2×2 propagation matrix T_j.

The fields in the jth section can be calculated from the known fields in the previous section as

$$\begin{pmatrix}F_j\\R_j\end{pmatrix}=T_j\begin{pmatrix}F_{j-1}\\R_{j-1}\end{pmatrix}. \tag{7}$$

The propagation matrix for the jth mode has the form

$$T_j=\begin{pmatrix}\cosh(\gamma_j\Delta z)-i\frac{\sigma_j}{\gamma_j}\sinh(\gamma_j\Delta z) & -i\frac{\kappa_j}{\gamma_j}\sinh(\gamma_j\Delta z)\\ -i\frac{\kappa_j}{\gamma_j}\sinh(\gamma_j\Delta z) & \cosh(\gamma_j\Delta z)+i\frac{\sigma_j}{\gamma_j}\sinh(\gamma_j\Delta z)\end{pmatrix}, \tag{8}$$

where the coupling coefficients are related as

$$\gamma_j^2=\kappa_j^2-\sigma_j^2. \tag{9}$$

Note that the values of κ_j, σ_j and hence γ_j are different for each section and must be calculated individually before substituting into the propagation matrix.

The losses in the fibre and grating can be neglected because the latter is a few centimeters long.

The coupling coefficient is assumed Gaussian [10]

$$\kappa(z)=\kappa_p\exp\left(-\frac{4\ln2}{\Delta_\kappa^2}z^2\right), \tag{10}$$

where κ_p is the maximum value of the coupling coefficient and Δ_κ is the full width at half maximum (FWHM) of this distribution and is assumed equal to $L_{gr}/3$ in all calculations [10] (L_{gr} is the grating length).

The variations of the forward and backward fields can be found over a uniform cavity section by the transfer matrix method. The laser cavity is divided into sections with the equal effective length Δz. For the time step $\Delta t=\Delta z/v_g$ (v_g is the group velocity in the cavity), the forward and backward fields are calculated from the transfer matrix. In each laser section, the carrier density is calculated from the rate equation

$$\frac{dN(z,t)}{dt}=\frac{I(t)}{eV}-N(z,t)[A+BN(z,t)+C_AN(z,t)^2]$$

$$-\frac{a_0[N(z,t)-N_0]}{1+\varepsilon P(z,t)}v_gS(z,t)+F_N, \tag{11}$$

where $I(t)$ is the injection current; V is the active layer volume; P is the photon density; e is the electron charge; A is the nonradiative recombination constant in s^{-1}; B is the radiative recombination coefficient [which lies in the range of $(0.7-1.5)\times10^{-10}$ cm^3 s^{-1}]; and C_A is the Auger recombination coefficient in cm^6 s^{-1}. The measured values of C_A lie in the range of $(1-7.5)\times10^{-29}$ cm^6 s^{-1} for conventional InGaAsP lasers and they are higher for quantum-well structures. For this reason, we use $C_A=10\times10^{-29}$ cm^6 s^{-1} in this work. $S(z,t)$ is the photon density and it is proportional to $|F|^2+|R|^2$; N_0 is the carrier density upon transparency; ε is the gain saturation parameter; a_0 is the differential gain. In the simulation, the initial value 1.9×10^{18} cm^{-3} of carrier density was used; F_N is the carrier density fluctuations.

The carrier density fluctuations F_N cause the noise processes of two types [11]

$$F_N(z,t)=F_{nr}(z,t)-F_s(z,t). \tag{12}$$

The first term F_{nr} in the right-hand side of (12) describes the injection current noise and the noise caused by nonradiative recombination of carriers. This noise term is not correlated with the spontaneous emission process and is a Gaussian white noise with the correlation [11]:

$$\langle F_{nr}(z,t)F_{nr}(z',t')\rangle = (I/eV + N/\tau_n)\delta(t-t')\delta(z-z') \quad (13)$$

Thus, the first term in (13) determines the injection current noise and it is neglected for this analysis. The second term F_s in the right-hand side of (12) results from radiative recombination and is therefore correlated to the spontaneous emission. In fact, since every emitted photon implies the recombination of one electron-hole pair, the carrier density noise resulting from photon emission is proportional to the fluctuation of the optical intensity.

The autocorrelation for $F_N(z,t)$ and the cross correlation between $F_N(z,t)$ and $S(z,t)$ become

$$\langle F_N(z,t)F_N(z',t')\rangle =$$

$$\left[\frac{I}{qV} + \frac{N}{\tau_n} + \frac{a_0(N-N_0)}{1+\varepsilon P}\upsilon_g P\right]\delta(t-t')\delta(z-z') \quad (14)$$

and

$$\langle F_N(z,t)S(z',t')\rangle =$$

$$-\beta_{sp}R_{sp}\frac{a_0(N-N_0)}{1+\varepsilon P}P\delta(t-t')\delta(z-z'), \quad (15)$$

respectively.

The change in the carrier density in laser sections causes the change in the refractive index:

$$\Delta n = -\frac{\lambda_0}{4\pi}\Gamma\alpha a_0 \Delta N(z,t), \quad (16)$$

where Γ is the optical confinement factor; α is the linewidth broadening factor; and $\Delta N(z,t)$ is the change in the carrier density.

For each time step Δt, the new field values are calculated taking the boundary conditions into account. The small-signal IM response function $H(f)$ is the ratio of the small-signal photon density ΔS to the small-signal injection current ΔI [12–14].

$$H(f) = \frac{\Delta S}{\Delta I}. \quad (17)$$

This can also be written in terms of the power modulation

$$H(f) = \frac{\Delta P_{out}}{\Delta I}. \quad (18)$$

The RIN is determined as the relative fluctuation power from the expression

$$\frac{\mathrm{RIN}(f)}{\Delta f} = \frac{2\langle|\Delta S(w)|^2\rangle}{\langle S\rangle^2}\,(\mathrm{dB\ Hz^{-1}}), \quad (19)$$

where $\langle S\rangle$ is the average optical power; $\Delta S(w)$ is the spectral noise density in the bandwidth Δf at a specified frequency. Note that the effective bandwidth is $2\Delta f$ since we must include both positive and negative frequencies.

3. Results and discussion

We calculated the HSPS with a linearly chirped Gaussian apodised FBG with the maximum power reflectivity of 0.5 at 1.55 μm. The linear chirp coefficient C is -1.9 Å cm^{-1}. A laser diode of length 250 μm and a FBG length 4 cm were used. The fundamental frequency of the cavity was taken to be 2.5 GHz. The other MQW laser diode parameters are given below. The values of these parameters are close to real values [6].

Gain saturation parameter $\varepsilon/\mathrm{cm^3}$	2×10^{-17}
Slope gain $a_0/\mathrm{cm^2}$	10×10^{-16}
Spontaneous emission factor β_{sp}	5×10^{-5}
Line broadening factor α	2
Cavity field coupling coefficient η	0.8
AR coating reflectivity r_3	0.01
HR coating reflectivity r_1	0.9
Optical confinement factor Γ	0.1
Nonradiative recombination coefficient $A/\mathrm{s^{-1}}$	4×10^{8}
Bimolecular recombination coefficient $B/\mathrm{cm^3\ s^{-1}}$	10^{-10}
Auger recombination coefficient $C_A/\mathrm{cm^6\ s^{-1}}$	10×10^{-29}
Internal losses $\alpha_{int}/\mathrm{cm^{-1}}$	25
Carrier density upon bleaching $N_0/\mathrm{cm^{-3}}$	1.2×10^{18}
Time step $\Delta t/\mathrm{ps}$	0.6875
Threshold current I_{th}/mA	3.2

The model simulates the HSPS generating 50–80-ps pulses of at a pulse repetition rate of 2.488 GHz for use in soliton communication systems [1, 6]. The FBG has a very small linear chirp to produce long optical pulses, and has a narrow bandwidth providing a good wavelength control.

It is known that if the modulation frequency of a conventional mode-locked system is changed from the specified frequency, mode-locking cannot be obtained. In order to see whether the HSPS is properly mode-locked or not, the field spectrum, the width of output pulses and their time-bandwidth products (TBP) are examined for transform-limited pulses, which should correspond to soliton type pulses.

The results of our calculations show that in the absence of noise or taking into account only spontaneous noise, the HSPS generates nearly transform-limited pulses tunable in the range from 2 to 3 GHz near the fundamental frequency 2.5 GHz although the RIN spectrum has a maximum at the fundamental frequency [7, 15]. This tuning range obtained in [6] was 850 MHz.

If only the carrier density noise is taken into account, the RIN maximum is located at the mode-locking frequency of 2.3 GHz and is equal to -96.97 dB Hz^{-1} (Fig. 2a). The corresponding output pulse is given in Fig. 2b. One can see that the TBP becomes meaningless for signals for which its value is 0.007. This value does not satisfy the condition of a transform-limited pulse and therefore the pulse is not a soliton. Transform-limited pulses were not obtained also at the mode-locking frequency of 2.1 GHz at which the TBP is 0.601. Thus the carrier density fluctuations affect the output pulse of mode-locked HSPSs more than the spontaneous noise. It was pointed out in [16] that the noise of a mode-locked laser is different from that of solid-state lasers, such as fibre lasers, Nd^{3+} : YAG lasers, Ti : sapphire lasers, and others with the slow gain dynamics. The difference stems from the fact that carrier lifetime is very short for mode-locked lasers and hence the effect of the gain fluctuations on

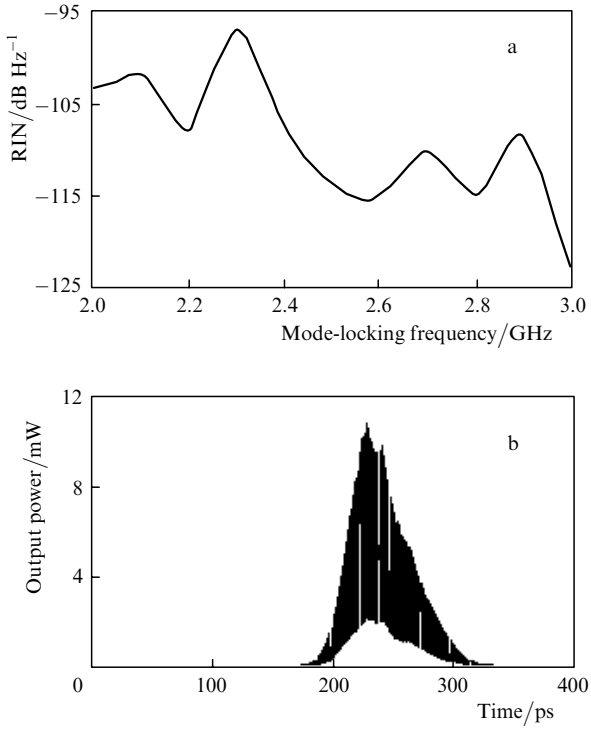

Figure 2. Relative intensity noise spectrum of the mode-locked HSPS (a) and the output power of the mode-locked HSPS at the frequency 2.3 GHz (b) taking into account only the carrier density noise.

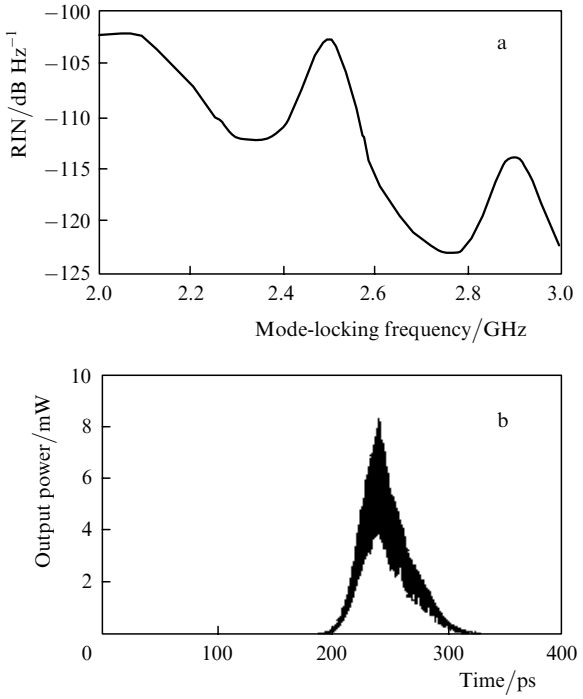

Figure 3. Relative intensity noise spectrum of the mode-locked HSPS (a) and the output power of the mode-locked HSPS at the frequency 2.3 GHz (b) taking into account the spontaneous noise and carrier density noise.

the pulse timing is important already on a round-trip time scale. The effect of carrier density fluctuations on the time jitter was also studied in [17, 18]. All these results show the importance of the carrier density noise in mode-locked lasers.

The RIN has a maximum of -102.90 dB Hz^{-1} at the fundamental mode-locking frequency of 2.5 GHz if both the spontaneous and carrier density noise is taken into account (Fig. 3a). Transform-limited pulses are not generated at this frequency because the TBP is 0.011. The output pulse at the frequency 2.5 GHz is shown in Fig. 3b. Small fluctuations in the carrier density lead to small fluctuations in the field amplitude. However, negative feedback due to stimulated emission modulating the carrier density tends to suppress amplitude fluctuations. For this reason, the noise decreases especially near the fundamental mode-locking frequency, when the HSPS has both the spontaneous and carrier density noise (sf. Figs 2a and 3a).

The calculations show that, if standard laser diode parameters presented above are used, an increase in the RIN leads to the narrowing of the frequency range of pulses down to 800–900 MHz in the presence of only the carrier density noise or both the spontaneous and carrier density noise (Figs 2a and 3a). The high noise level of the device observed at frequencies 2.3 GHz (Fig. 2a) and 2.5 GHz (Fig. 3a) resulted in a low signal-to-noise ratio. This explains why transform-limited pulses cannot be obtained at these frequencies. Furthermore, as β_{sp} increases, the RIN becomes greater in a broad spectrum of the mode-locking frequencies, and mode-locking is difficult to achieve. Therefore, transform-limited pulses are not generated over a wide tuning range regardless of the type of noise in the HSPS.

The RIN spectra for different β_{sp} taking into account both the spontaneous and carrier density noise are presented in Fig. 4. In this case the RIN maximum is located at the mode-locking frequency 2.5 GHz at which transform-limited pulses are not generated at any value of β_{sp} (Table 1). Note that transform-limited pulses are also not generated at the mode-locking frequencies 2 GHz for $\beta_{sp} = 10 \times 10^{-5}$ and 2 and 2.4 GHz for $\beta_{sp} = 20 \times 10^{-5}$. However, as follows from Table 1, for $\beta_{sp} = 20 \times 10^{-5}$ these pulses are not generated only at the fundamental mode-locking frequency if only the spontaneous noise is considered [7, 15].

Active mode locking is a resonance phenomenon at which the laser is modulated at a frequency corresponding to the inverse round-trip transit time of the laser cavity. For this reason, the RIN spectrum has a noise maximum at the

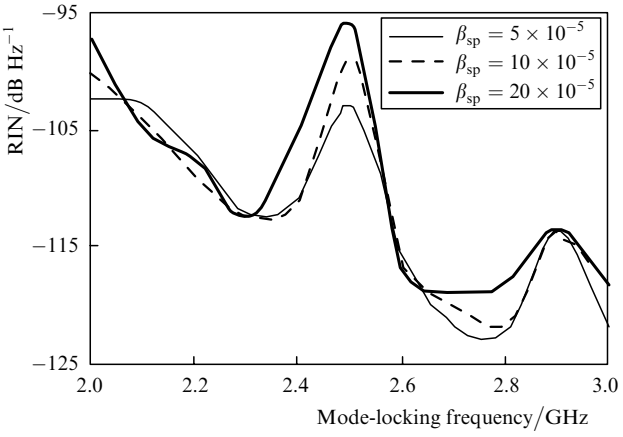

Figure 4. Relative intensity noise spectra of the mode-locked HSPS for different β_{sp} taking into account the spontaneous noise and carrier density noise.

Table 1. Influence of the value of β_{sp} in a linearly chirped Gaussian apodised FBG at the mode-locking frequency 2.5 GHz.

$\beta_{sp}/10^{-5}$	Δ_k/ps	Spectral width/GHz	TBP
5	45.38/40.55*/1.278**	8.68/8.60*/8.80**	0.394/0.349*/0.011**
10	45.47/32.53*/0.963**	8.71/8.68*/8.81**	0.396/0.282*/0.008**
20	45.60/3.98*/0.775**	8.73/8.98*/8.69**	0.398/0.036*/0.007**

Note: *taking the spontaneous noise into account; ** taking the spontaneous noise and carrier density noise into account.

resonance frequency which shows the optical resonance due to the cavity round-trip transit time. However, Fig. 2a shows that this is not the case. The noise peak shifts to the red, resulting in the dependence of the wavelength on the number of photons in the active region.

The obtained results show that the carrier density noise is as important as the spontaneous noise in lasers. It affects the output pulse of a mode-locked HSPS and inclusion of this noise in the rate equations is necessary for accurate analysis of the noise. These results also show that transform-limited pulses can be obtained over a wide frequency range if the RIN is smaller than -103 dB Hz^{-1}.

Figure 5 shows the calculated IM response of the HSPS in the frequency range from 0.1 GHz to 20 GHz at a forward bias current of 6 mA. The fundamental peak amplitude is approximately greater by 4 dB than the response amplitude at low frequencies, in good agreement with calculated and measured IM responses reported in [3]. The first order peak is slightly shifted to the blue with respect to the cavity frequency of 2.5 GHz, as in [5]. The first resonance has no RPSS if standard laser diode parameters are used in calculations. The origin of the amplitude discontinuity was investigated in [3–5], where it was shown that the high reflectivity r_3 of the AR coating, a weak coupling η between active and passive cavities, a low gain compression factor ε, the linewidth broadening factor α, and the external cavity length have a significant effect on the RPSS.

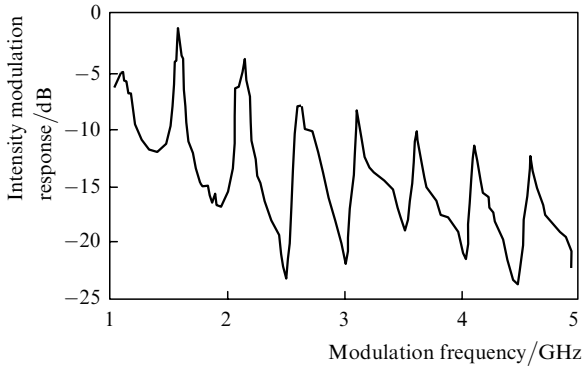

Figure 5. Frequency characteristic of the intensity modulation for the HSPS with a linearly chirped FBG.

Now, we will investigate the IM of the HSPS in the frequency range from 1 GHz to 5 GHz for different values of device parameters.

The external cavity length: Figure 6 shows the IM spectra of the HSPS for external cavity lengths of 2, 4 and 5.5 cm. One can see that the amplitude and bandwidth of the IM spectra depend on the cavity length and the IM spectra are continues for cavity lengths 2 and 4 cm. Our

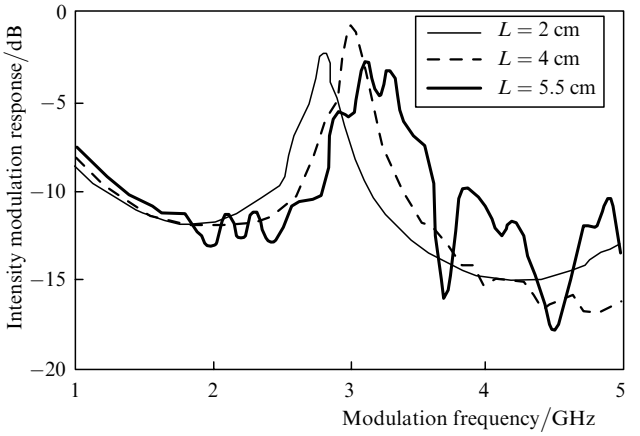

Figure 6. Effect of the external cavity length L on the intensity modulation response.

calculations also show that the cavity length must be shorter than 4.5 cm to obtain a good IM response from the HSPS with a linearly chirped Gaussian apodised FBG. These results indicate, as results [4], that the external cavity length considerably affects the IM spectra.

The AR coating reflectivity r_3: To estimate the effect of the AR coating reflectivity on the irregularity and modulation bandwidth, we performed calculations for different values of r_3. We found that the irregularity was insignificant for different r_3, while the modulation bandwidth was minimal for the standard value of r_3. The irregularity was almost absent at low r_3, and for $r_3 = 0$ a continues response can be obtained [3]. These results show that the AR coating weakly affects the RPSS if a linearly chirped Gaussian apodised FBG is used as the external cavity.

The field coupling factor η: Although the right facet of the laser diode is AR coated to provide the maximum light coupling to the fibre, its transmission is not perfect, and the reflection coefficient of the AR coating is taken as 0.01 in practice. In addition, due to the laser–fibre interface (splicing losses), the light field cannot completely transfer from the laser to fibre and vice versa. The splicing losses in our model are described by the coupling factor η, which is assumed to be 0.8 for both laser-to-fibre and fibre-to-laser light field transfer.

Figure 7 shows the IM response for a strong ($\eta = 0.8$) and weak ($\eta = 0.2$) optical feedback. One can see that the IM irregularity disappears for $\eta = 0.8$. In [3], it was also pointed out that the irregularity was almost completely suppressed in the case of a strong feedback, which possibly increases the damping of the high-frequency peak thereby enhancing its wings. Note that the amplitude irregularity appears near the cavity resonance frequency. The response amplitude increases in a broader peak corresponding to the high-frequency peak, while the narrower peak corresponds to the low-frequency peak [3]. As pointed out before, the external cavity of the HSPS consists of an AR coated lens-like fibre end spliced to a section of a photosensitive fibre with the induced Bragg reflector, which provides the efficient coupling of a laser diode with a fibre [19]. One can see from Fig.7 that the coupling factor has also strong effect on the magnitude and bandwidth of the IM response, the amplitude increasing with increasing η.

The optical confinement factor Γ: Because not all stimulated emission or the field in the laser cavity is confined

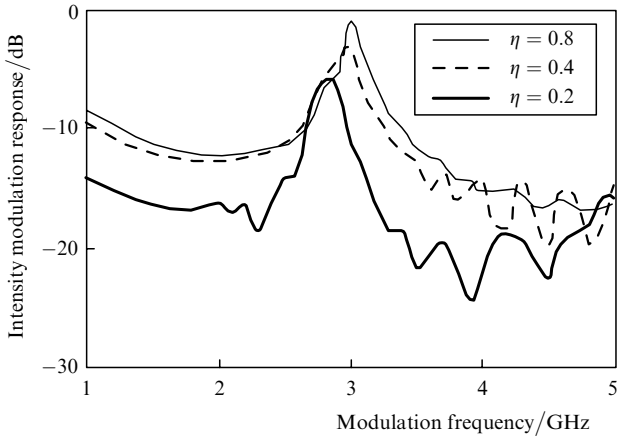

Figure 7. Effect of the cavity field coupling η on the intensity modulation response.

within the active region of the laser, the optical confinement factor Γ is introduced. Conventional lasers with the Fabry–Perot cavity have the confinement factor $\Gamma = 0.2 - 0.4$, depending on the structure and dimensions of the laser diode. MQW lasers have lower confinement factors (typically 0.1 or less) due to their very small active region sizes, therefore, we assumed here that $\Gamma = 0.1$. The resonance peak shifts to the blue and its amplitude increases with Γ as shown in Fig. 8, because Γ is the fraction of the mode energy contained in the active region. As Γ increases, the mode energy within the active region and, hence, the optical gain increases. The modulation bandwidth is small for the standard value of Γ. The value of Γ considerably affects the IM response.

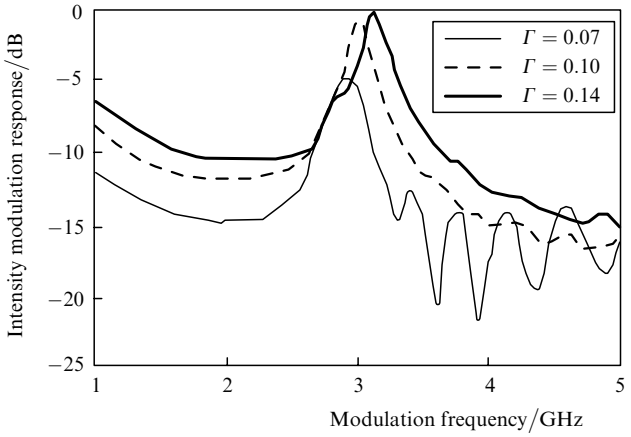

Figure 8. Effect of the optical confinement factor Γ on the intensity modulation response.

The gain saturation factor ε*:* The gain saturation is an important effect in semiconductor lasers, especially in InGaAsP lasers. The gain saturation is caused by spatial inversion hole burning, spectral hole burning and other nonlinearities. Spatial hole burning can be neglected in high-speed InGaAsP lasers due to the dominant effect of spectral hole burning. Spectral hole burning give rise to the power-dependent gain. The power-dependent gain has been used to explain the experimental red shift of the dominant mode with increasing the laser current.

We studied the IM in the HSPS for $\varepsilon = 0$, 2×10^{-17} and 4×10^{-17} cm^3. The modulation amplitude decreased approximately by 2.5 dB when ε was changed from 0 to 4×10^{-17} cm^3. The resonance peak amplitude can decrease due to a stronger decay relaxation oscillations [20], and a stronger decay of the high-frequency peak [3] caused by a strong nonlinear gain saturation. The modulation bandwidth increased with increasing ε, as in [3]. Although the value of ε affects the IM amplitude and bandwidth, its influence on the RPSS in the IM spectra is insignificant.

The linewidth broadening factor α determines the spectral linewidth and frequency chirp. The value of α for MQW lasers is approximately half that for similar lasers with bulk active layers, and therefore, we assume that $\alpha = 2$. In semiconductor lasers, α determines the dependence of the refractive index on the carrier density. The IM response strongly depends on α (Fig. 9). As expected, the irregularity of the IM response disappears at large α. Although the modulation bandwidth is maximal for $\alpha = 0$, its amplitude decreases approximately by 2.3 dB. These results, as [4, 5], show that α considerably affects the RPSS.

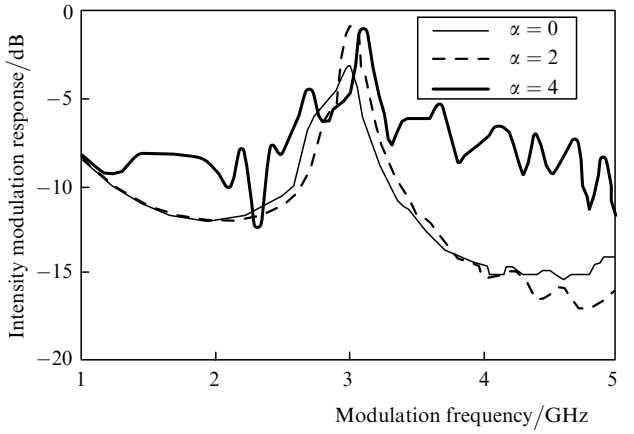

Figure 9. Effect of the linewidth broadening factor α on the intensity modulation response.

The spontaneous emission factor β_{sp}*:* Spontaneous recombination events supply photons into the lasing field, the fraction of these photons being determined by the spontaneous emission factor β_{sp}. This factor is important for the laser dynamics; for $\beta_{sp} = 0$ and $S = 0$ at $t = 0$, the photon density S would remain zero. The effect of this parameter on the IM response is very small: the IM response amplitude increases weakly with increasing β_{sp}.

The nonradiative recombination coefficient A noticeably affects the IM amplitude and bandwidth (Fig. 10). The amplitude decreases and the bandwidth increases with increasing A. The resonance peak shifts to the blue with decreasing A.

The bimolecular recombination coefficient B: As B increases up to 1.5×10^{-10} cm^3 s^{-1}, the resonance peak intensity slightly increases and the bandwidth decreases (Fig. 11). However, for $B = 2 \times 10^{-10}$ cm^3 s^{-1}, the resonance peak decreases approximately by 3 dB and its bandwidth increases compared to that for $B = 1 \times 10^{-10}$ cm^3 s^{-1}. This occurs because the radiative recombination rate is proportional to the square of the carrier density in the active region.

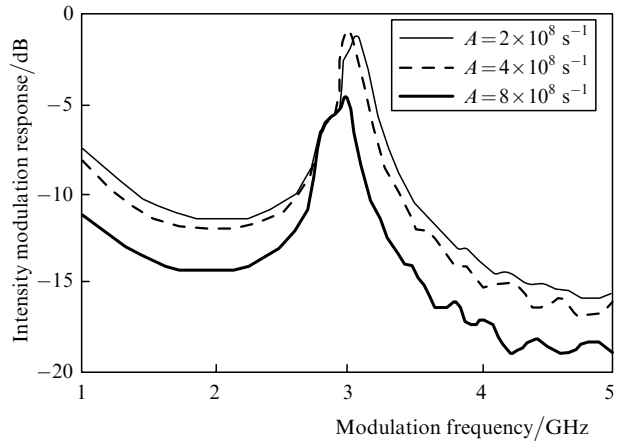

Figure 10. Effect of the nonradiative recombination coefficient A on the intensity modulation response.

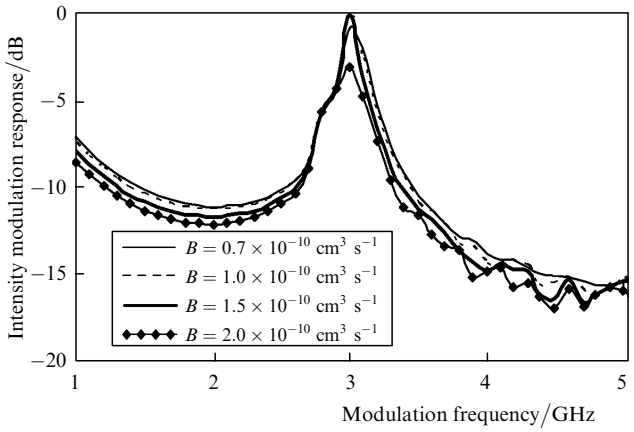

Figure 11. Effect of the bimolecular recombination coefficient B on the intensity modulation response.

The Auger recombination coefficient C_A is proportional to the cube of the carrier density. If it is increased, the carrier density in the active region decreases and, hence, the optical gain also decreases, which is confirmed by our results. Figure 12 shows that the response amplitude decreases and the bandwidth increases with increasing C_A, while the resonance peak shifts to the red. This shift occurs because a decrease in the carrier density leads to an increase in the refractive index, resulting in the increase in the emission wavelength (or the decrease in the emission frequency).

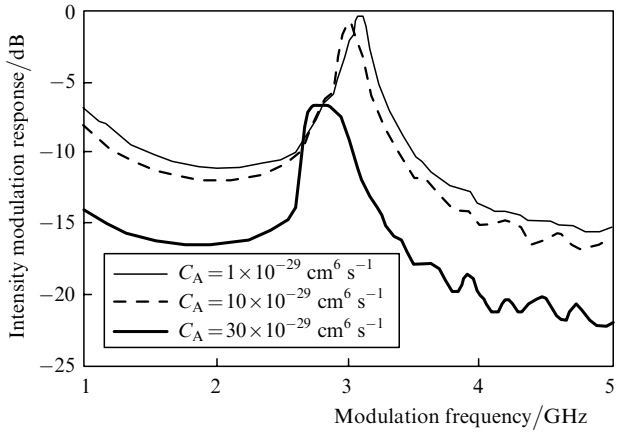

Figure 12. Effect of the Auger recombination coefficient C_A on the intensity modulation response.

The forward bias current: As the forward bias current increases, the resonance IM peak shifts to the blue and the modulation bandwidth also increases (Fig. 13) [3]. Similar behaviour of the response was predicted theoretically and observed experimentally [3]. The increase in the modulation bandwidth of the resonance peak with increasing the forward bias current is caused by damping enhanced due to the nonlinear gain saturation [3]. Note also that if laser diode is biased close to the mode-hopping region, the IM spectrum splits (Fig. 13b). Thus, these results show that the forward bias current considerably affects the RPSS in the IM response.

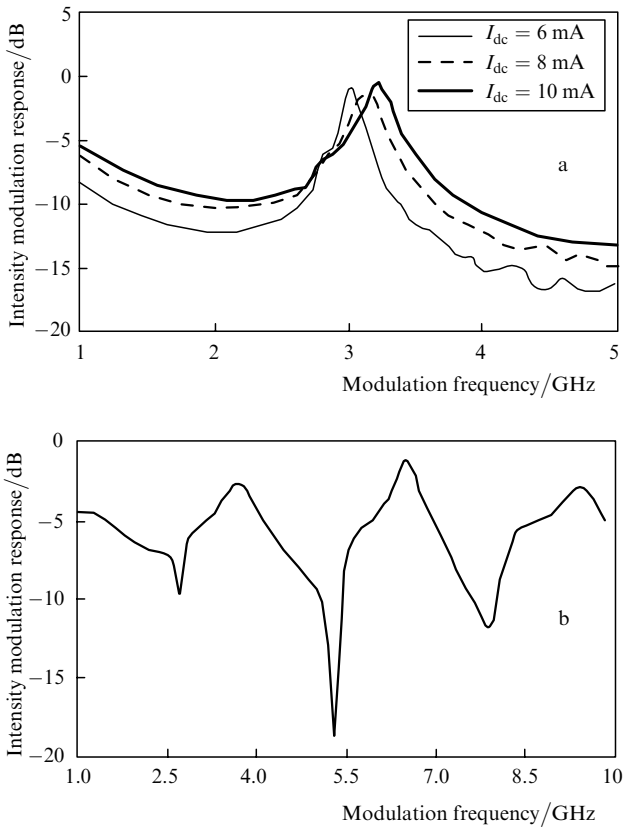

Figure 13. Effect of the direct current I_{dc} on the intensity modulation response (a) and on the intensity modulation response of the HSPS for the current $I_{dc} = 22$ mA (b).

The chirp rate C: The results obtained up to now show that the RPSS in the IM response can be suppressed in the HSPS using linearly chirped FBGs and standard laser diodes. However, the RPSS appears near the fundamental frequency of 2.5 GHz for the HSPS with a Gaussian apodised FBG. The IM response in the frequency range of 1 – 5 GHz is shown in Fig. 14. The reason for the RPSS disappearance is the use of the appropriate linear chirp rate in the Gaussian apodised FBG. The chirp in the fibre allows the HSPS to operate in a broad mode-locking frequency range [1, 6]. This is an important feature for mode-locking

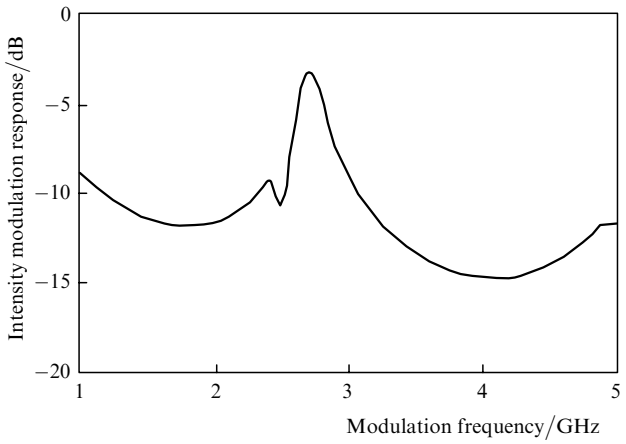

Figure 14. Intensity modulation response of the HSPS with a Gaussian apodised FBG.

applications because a laser can be mode-locked in a broad frequency range without changing the grating length. As the chirp is increased, the spectrum broadens and the side peak disappears. Although the group delay curve for an unchirped mirror is nonlinear, it becomes linear as the rate of chirp is increased. Therefore, strongly chirped gratings are most sutable for HSPS applications. We used in our simulation a grating length of 4 cm with a chirp rate of -1.9 Å cm^{-1} in order to obtain a broad mode-locking frequency range.

The IM responses obtained for different chirps are shown in Fig. 15. For the chirp rate equal to -1 and -3 Å cm^{-1}, the modulation bandwidth is greater and the resonance peak is weaker that for -1.9 Å cm^{-1}. In addition, for $C = -1$ and -3 Å cm^{-1}, the spectral splitting takes place near the fundamental frequency, which is absent for $C = -1.9$ Å cm^{-1}. The resonance peak shifts to the frequency 3.1 GHz at the chirp rate of -3 Å cm^{-1}.

Our simulation also show that the modulation bandwidth increases and the amplitude decreases as the number of harmonics of the resonance frequency increases (Fig. 5). The same behaviour was observed in [3]. These results lead to the important conclusion that the maximum bandwidth and the most intense resonance peak cannot be obtained simultaneously. Although the most intense resonance peak can be obtained near the fundamental resonance frequency of the external laser cavity, the modulation bandwidth will be small. A greater bandwidth can be obtained by using the modulation at higher harmonics of the resonance frequency, where resonance peaks are weaker.

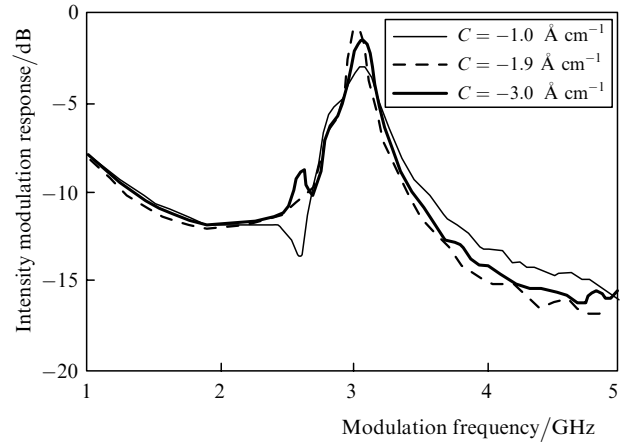

Figure 15. Effect of the chirp rate C on the intensity modulation response.

4. Conclusion

We have studied the RIN and small-signal IM response of an HSPS with a linearly chirped Gaussian apodised FBG. If the noise is neglected, the transform-limited pulses are generated over a broad tuning range of 1 GHz near the fundamental mode-locking frequency. The consideration of the spontaneous and carrier noise causes an increase in the RIN, especially at large spontaneous emission factors. The high RIN reduces the mode-locking range where transform-limited pulses can be generated.

It is shown that fluctuations of the carrier density affect the gain dynamics, and this should be taken into account by describing the noise of a semiconductor mode-locked laser. Therefore, the carrier density noise should be included in the rate equations along with the spontaneous noise in the HSPS when describing the noise characteristics of the mode-locked HSPS.

It is shown that the gain saturation factor, the AR coating reflectivity, the nonradiative recombination coefficient, the bimolecular recombination coefficient and the Auger recombination coefficient affect only the IM amplitude and bandwidth. The external cavity length, the field coupling efficiency, the optical confinement factor, the linewidth broadening factor and the forward bias current in the regime close to the mode-hopping regime strongly affect the irregularity of the IM spectrum, as well as the IM amplitude and bandwidth. In addition, we have shown that the RPSS can be removed by using an appropriate linear chirp rate in a Gaussian apodised FBG.

References

1. Morton P.A., Mizrahi V., Andrekson P.A., Tanbun-Ek T., Logan R.A., Lemaire P., Coblentz D.L., Sergent A.M., Wecht K.W., Sciortino P.F. Jr. *IEEE Photonics Techn. Lett.*, **5** (1), 28 (1993).
2. Paoletti R., Bertone D., Fang R., Magnetti G., Meliga M., Meneghini G., Morello G., Rossi G., Tallone L., Scofet M. *IEEE Photonics Techn. Lett.*, **12**, 245 (2000).
3. Ahmed Z., Tucker R.S. *IEEE J. Select. Topics Quantum Electron.*, **1** (2), 505 (1995).
4. Premaratne M., Lowery A.J., Ahmed Z., Novak D. *IEEE J. Select. Topics Quantum Electron.*, **3** (2), 290 (1997).
5. Pittoni F., Gioannini M., Montrosset I. *IEEE J. Select. Topics Quantum Electron.*, **7** (2), 280 (2001).
6. Ozyazici M.S., Morton P.A., Zhang L.M., Mizrahi V. *IEEE Photon. Techn. Lett.*, **7**(10), 1142 (1995).
7. Dogru N., Ozyazici M.S. *Opt. Quantum Electron.*, **35** (2), 169 (2003).
8. Dogru N., Ozyazici M.S. *IEEE Proc. Optoelctron.*, **150** (4), 346 (2003).
9. Kogelnik H., Shank C.V. *J. Appl. Phys.*, **43** (5), 2327 (1972).
10. Erdogan T. *J. Lightwave Techn.*, **15** (8), 1277 (1997).
11. Tromborg B., Lassen H.E., Olesen H. *IEEE J. Quantum Electron.*, **30** (4), 939 (1994).
12. Glasser L.A. *IEEE J. Quantum Electron.*, **16**, 525 (1980).
13. Lau K.Y. *IEEE J. Quantum Electron.*, **26**, 250 (1990).
14. Helms K. Peterman J. *J. Lightwave Techn.*, **9**, 468 (1991).
15. Dogru N., Ozyazici M. S. *Opt. Laser Techn.*, **35** (3), 163 (2003).

16. Jiang L.A., Grein M.E., Haus H.A., Ippen E.P. *IEEE J. Select. Topics Quantum Electron.*, **7** (2), 159 (2001).
17. Haus H.A., Mecozzi A. *IEEE J. Quantum Electron.*, **29** (3), 983 (1993).
18. Von der Linde D. *Appl. Phys. B*, **39**, 201 (1986).
19. Morton P.A., Mizrahi V., Kosinski S.G., Mollenauer L.F., Tanbun-Ek T., Logan R.A., Coblentz D.L., Sergent A.M., Wecht K.W. *Electron. Lett.*, **28** (6), 561 (1992).
20. Manning J., Olshanksy R., Fye D.M., Powazinik W. *Electron. Lett.*, **21**, 496 (1985); Adams M.J., Osinski M. *Electron. Lett.*, **19**, 627 (1983).